



Maskless lithography for large area patterning of three-dimensional microstructures with application on a light guiding plate

YONG-SIN SYU,¹ YU-BIN HUANG,² MING-ZE JIANG,¹
CHUN-YING WU,¹ AND YUNG-CHUN LEE^{1,*}

¹Department of Mechanical Engineering, National Cheng Kung University, Tainan 701, Taiwan

²ASML Tainan, Tainan City 744002, Taiwan

*yunglee@mail.ncku.edu.tw

Abstract: This paper presents a maskless lithography system that can perform three-dimensional (3D) ultraviolet (UV) patterning on a photoresist (PR) layer. After PR developing processes, patterned 3D PR microstructures over a large area are obtained. This maskless lithography system utilizes an UV light source, a digital micromirror device (DMD), and an image projection lens to project a digital UV image on the PR layer. The projected UV image is then mechanically scanned over the PR layer. An UV patterning scheme based on the idea of obliquely scanning and step strobe lighting (OS³L) is developed to precisely control the spatial distribution of projected UV dose, such that desired 3D PR microstructures can be obtained after PR development. Two types of concave microstructures with truncated conical and nozzle-shaped cross-sectional profiles are experimentally obtained over a patterning area of 160 × 115 mm². These patterned microstructures are then used for replicating nickel molds and for mass-production of light-guiding plates used in back-lighting and display industry. Potential improvements and advancements of the proposed 3D maskless lithography technique for future applications will be addressed.

© 2023 Optica Publishing Group under the terms of the [Optica Open Access Publishing Agreement](#)

1. Introduction

Photolithography plays a key role in micro/nano-manufacturing with a wide range of applications and far-reaching importance in modern industry. Conventional photolithography methods use a photomask to define and pattern a thin layer of photosensitive polymer material, known as photoresist (PR), which is spin-coated on a substrate. Ultraviolet (UV) light passing through a photomask is then projected onto the photoresist layer for UV exposure. After being soaked in a chemical developer, a patterned PR layer is formed by chemical etching reaction, which is known as PR developing process. The patterned PR layer is then used for subsequent material processing on the substrate. To cope with different feature sizes and complexities in the required PR patterns, the fabrication of photomasks can be challenging, time-consuming, and expensive. As a result, various techniques for maskless lithography have been developed. For example, there is electron beam lithography [1,2], laser direct writing [3–5], or combining different forms of optical elements, such as optical diffraction elements and light modulators to miniaturize ultraviolet light into tiny spots and cooperate with mechanical scanning to complete the definition of micro-patterns [6–8].

Recent developments and advancements in digital light processing (DLP) technologies have provided a new methodology for maskless lithography. The key element in DLP is the digital micromirror device (DMD) developed by Texas Instruments Inc. (Dallas, Texas, USA) [9]. A DMD chip composes of a rectangular array of micromirrors that are driven by LVCMOS electronic circuits. The micromirrors can be in two tilted positions of ±12° depending on the ON or OFF voltage status of their corresponding LVCMOS circuits. In this way, a digital and binary image can be formed by a DMD chip and each micromirror is a pixel of the image. There are a

lot of applications such as projectors, 3D printing systems, spatial light modulators, etc. There are also many studies using DLP and DMDs for maskless lithography applications. For example, in 1999, Takahashi and Setoyama [10] used a DMD to develop an UV lithography system and successfully achieved 50 μm linewidth feature size on a 1.2 μm thick photoresist. Ren Yang et al. [11] and Kin Foong Chan et al. [12] developed and integrated a microlens and spatial filter array (MLSFA) in a DMD lithography system to improve the linewidth resolution to 1.5 μm .

Recently it is noticed that DMD-based maskless lithography not only can be used for patterning two-dimensional (2D) PR microstructures but also three-dimensional (3D) ones. In comparison to conventional photolithography using photomasks, DMD-based lithography can easily control the spatial distribution of UV dose exposed on a PR layer. Such capability of 3D UV patterning can create 3D microstructures on photoresist layers after PR development and has various important applications. Examples are light guide molds for backlight modules of flat panel monitors [13–16], GaN-based LED/OLED/LD surface structuring to improve light extraction efficiency of luminophores [17], microelectromechanical systems [18], micro-optical components [19–21], and so forth. There are already many methods to fabricate 3D microstructures, such as ultra-precision machining [19,22], laser micromachining [19,23], thermal reflow [24,25], and 3D printing [26]. However, on some occasions, DMD-based lithography has its own advantages in terms of smaller feature sizes, complicated and versatile 3D profiles, large patterning area size, and high throughput [27–29]. In the literature, there are already several 3D lithography based on different UV exposure methods, such as multi-layer exposure [30,31], inclined exposure [32–34], backside exposure of transparent substrates [35], large-area exposure with moving light sources [36], high-resolution grayscale lithography based on characteristic curve of photoresist [37–41], mask scanning exposure [42], and dose-controlled grayscale lithography with DMDs and MLSFA [43–46].

In reviewing all the 3D lithography methods mentioned above, this study proposed a new type of DMD-based lithography system and its working algorithm to fulfill 3D UV patterning on a PR layer. The goal is to achieve high resolution and high accuracy UV dose control. In the meantime, maintain the capabilities of large-area UV patterning and higher patterning speed. In Section II, both the hardware and software systems of the proposed maskless lithography method will be discussed in detail. Particular emphasis is placed on a new type of UV patterning scheme which relies on the synchronized coordination between the DMD chip, UV light source, and mechanical movement. Also introduced an algorithm for determining the optimized DMD images for fabricating microstructures with pre-designed surface profiles. In order to test and verify its capabilities in 3D lithography, the established maskless lithography system is applied to fabricate a mother mold which can be used for mass-production of light guiding plates. Experimental procedures and results will be discussed in detail in Section III. Conclusions and further developments and developments on the proposed DMD-based maskless lithography system are given in Section IV.

2. DMD-based maskless lithography system

2.1. Maskless lithography system

As shown in Fig. 1, the maskless lithography system developed in this study consists of several important components and sub-systems. It has an ultraviolet (UV) light source (3300B-651, Innovations in Optics, MA, USA) using high-power UV light-emitting diodes (LEDs). The light source has a center wavelength of 405 nm and maximum output power of 16 W when operating at 3 A electrical current. It can illuminate the DMD chip with an illuminance uniformity better than 95%. A reverse-type total internal reflector (RTIR) which consists of two prisms made of Schott N-SK16 optical glass transfers UV light from the light source to the DMD chip. A 0.7" DMD chip (DLP7000-0.7" XGA, TI, TX, USA) with an array of 1024×768 micromirrors (or pixels) and a pixel size of 13.68 μm is used in this maskless lithography system. The UV light enters the

DMD chip at an incident angle of 24° . So that, if a DMD micromirror is in the status of “ON”, the UV light will be reflected to the image projection lens as shown in Fig. 1. Otherwise, if a pixel is in the status of “OFF”, the UV light will be deflected to an optical absorber. In this manner, a digital image defined by the DMD chip can be projected through the image projection lens to a photoresist (PR) layer deposited on a substrate. The PR layer is placed at the image plane of the projection lens, or the x-y plane and the PR-coated substrate is carried by a servo-controlled multiaxial (x-y-z) motion stage. As shown in Fig. 1, the DMD-defined UV image projected on the x-y plane plays a dominant role in the UV patterning of the PR layer. The DMD chip is controlled by a DMD controller board (V-7001, ViALUX GmbH, Chemnitz, Germany) and can achieve a maximum frame rate of 22,727 Hz when operating with binary images. These binary images are sent to the DMD controller sequentially from a personal computer (PC) which acts as the controller and coordinator of the overall maskless lithography system. The system utilizes a high-resolution double-telecentric 0.5x imaging lens system (SL07, Sun Yang Optics Inc., Taoyuan City, Taiwan) designed for 405 nm wavelength with a 2" lens aperture and 0.125 numerical aperture (NA). The projected UV image thus contains an array of 1024×768 pixels with a pixel size of $6.84 \mu\text{m}$ (half of the DMD pixel size) and has a total UV exposure area size around $7.00 \times 5.25 \text{ mm}^2$. To achieve high-resolution and large-area UV patterning, the projected UV image is mechanically scanned over the entire PR-coated substrate. In the meantime, the digital images projected on the PR layer need to be continuously adjusted and simultaneously synchronized with the stage motion such that a desired spatial distribution of UV dose on the x-y plane can be achieved for 3D UV patterning of the PR layer. This requires a sophisticated UV patterning scheme to arrange and control both the hardware and software of the DMD-based maskless lithography system.

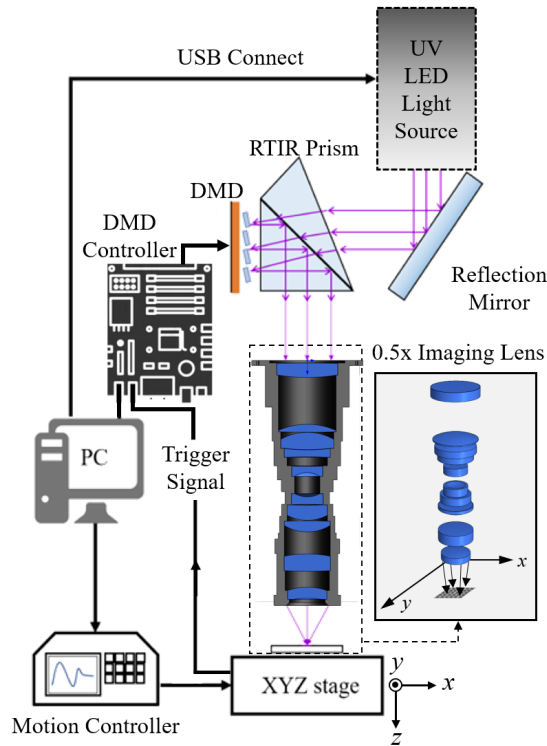


Fig. 1. Schematic illustration of the DMD-based maskless lithography system.

2.2. Irradiance of projected UV spots

To facilitate precise UV patterning, the optical intensity distribution of an UV spot projected from a DMD pixel at the x-y plan needs to be determined first. A high-resolution CMOS image sensor (UI-3594LE Rev.2, IDS Imaging Development Systems GmbH, Obersulm, Germany) is used for grayscale measurement of the projected intensity profile of an UV spot. This 1/2" CMOS image sensor composes of 4912×3684 pixels with a pixel size of $1.25 \mu\text{m}$, which gives an optical sensing area of $6.140 \times 4.605 \text{ mm}^2$. This grayscale image sensor is first working parallelly with a power meter (PD300, Ophir Optronics, Jerusalem, Israel) for measuring the DMD projected UV light at different optical power levels by adjusting the electrical current of the UV-LED light source from 0.1 A to 3.0 A in a step of 0.1 A. To avoid image saturating, the image sensor is covered with an optical attenuator with an optical density (OD) value of 3 and operated under a shutter time of 0.5 ms. Figure 2 shows the experimentally determined correlation between the irradiance measured from the power meter and the grayscale value measured from the image sensor. It showed good linearity when the grayscale is under 200 and therefore allowed the image sensor to direct measure the spatial distribution of irradiance.

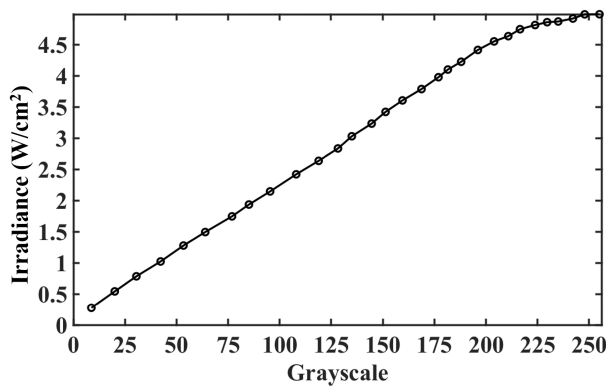


Fig. 2. Correlation between the projected irradiance of 405 nm UV light and the grayscale measured by the CMOS image sensor along with an attenuator of OD 3 and a shutter time of 0.5 ms.

The calibrated CMOS image sensor is now ready for measuring the optical intensity profile of a projected UV spot at the imaging plane. The electrical current of the UV-LED light source is kept at 3 A in this work. One single pixel of the DMD chip is turned ON while all the other pixels are OFF. The image sensor is then placed at the imaging plane by adjusting the z-axis of the motion stage. The measured grayscales of the single projected UV spot are then converted into irradiance based on the calibration data shown in Fig. 2. Finally, the irradiance of a projected UV spot on the x-y plane, the $I(x, y)$, is measured and shown in Fig. 3(a). It can be seen that in Fig. 3(a), due to the optical diffraction effect of the projection lens, the irradiance of a projected UV spot has a Gaussian distribution and can be modeled by,

$$I(x, y) = I_0 e^{-\frac{2(x^2+y^2)}{w_0^2}}. \quad (1)$$

where I_0 is the peak power intensity, and w_0 is the radius at 13.5% level of the peak intensity. The values of I_0 and w_0 are determined by the least squares fitting of Eq. (1) to the measured data and are obtained as 4.325 W/cm^2 and $4.64 \mu\text{m}$, respectively. Figure 3(b) and 3(c) show the modeled optical intensity profiles (solid lines) and measured data points of the UV spot along the x- and y-axis, respectively. Based on Eq. (1) and the modeled parameters, the diameter of the UV

spot size measured at the full width of half magnitude (FWHM) of its intensity profile is around $6.88 \mu\text{m}$, which is close to the projected DMD pixel size of $6.84 \mu\text{m}$.

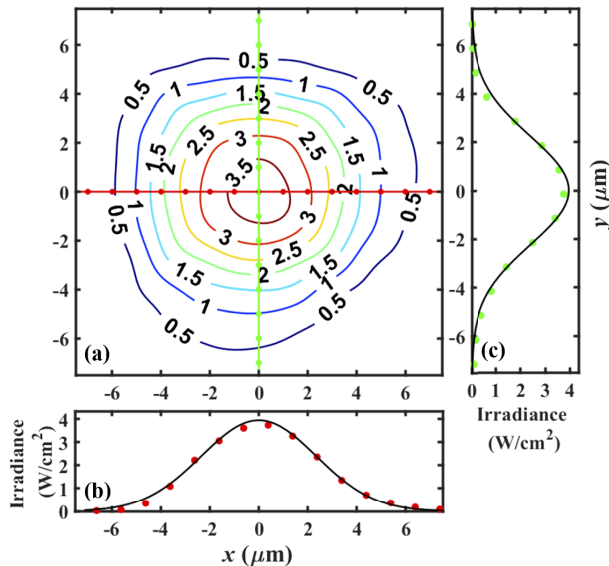


Fig. 3. (a) The contour plot of the measured intensity distribution of a projected UV spot, and (b) and (c) the cross-section plots of modeled Gaussian distribution of UV irradiance along the x- and y-axis, respectively.

2.3. UV patterning based on obliquely scanning and step strobe lighting (OS^3L)

The ultimate goal of a maskless lithography system is to precisely deliver a specific distribution of UV dose to expose a PR layer. Therefore, after developing processes, the developed PR microstructures can have the targeted 3D profiles. For DMD-based maskless lithography, there are many considerations that need to be taken into account when constructing such an UV patterning scheme. Examples are the smallest linewidth/line-spacing (L/S), pattern resolution and accuracy, the largest patterning area, and expected patterning speed or throughput. Some of these specifications are contradictory to each other and hence trade-offs are needed in constructing the UV patterning scheme.

In this study, we developed an UV patterning scheme for DMD-based maskless lithography based on an obliquely scanning and step strobe lighting (OS^3L) method. As shown in Fig. 4, an $M \times N$ array of UV spots with a pixel size of Δ is projected on the x-y plane and ready for UV patterning. Targeted UV patterning areas are shown in gray color and placed within the 1st quadrant of the x-y coordinate. To achieve better resolution in UV patterning, the projected UV spot array is deliberately tilted with an angle of θ with respect to the x-y coordinate. Ideally, the angle θ should be equal to or slightly bigger than $\arctan(1/N)$ to ensure that the scanning lines are nearly equally spaced. In the case of this work, N is 768 and the corresponding θ is 0.075° , which is very small. These UV spots of an oblique array are then scanned along the y-axis at a constant speed (v) while exposing the PR layer simultaneously under the command of digital DMD images. The width of the patterning area for one scan is very close to the width of the projected DMD array, which is $M \times \Delta$, and the scanning length can be arbitrarily long and only limited by the motion stage. Multiple scans can be carried out consecutively by shifting their positions on the x-axis and finally a large UV patterning area can be achieved in a pattern stitching manner.

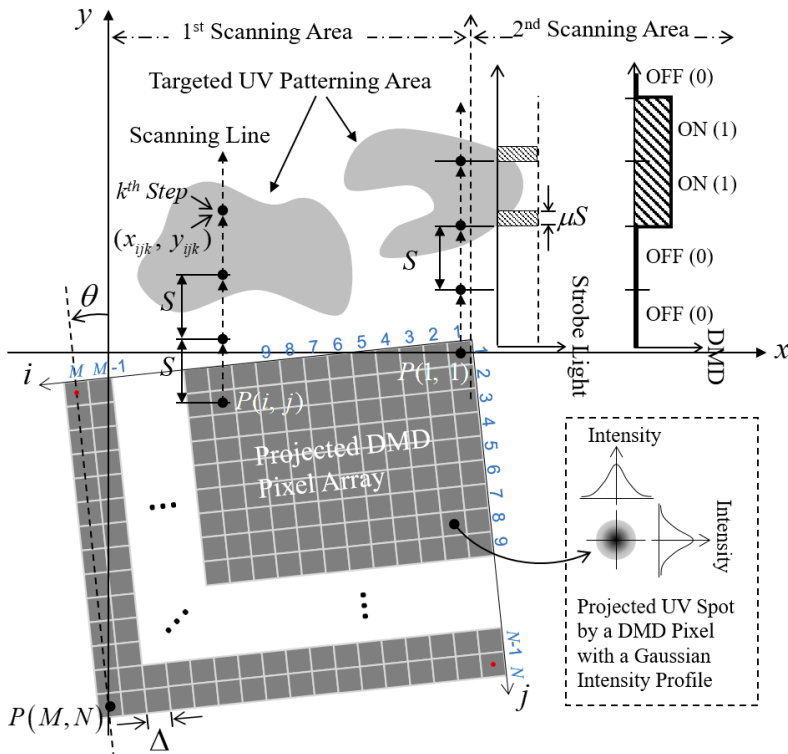


Fig. 4. Schematic diagram of the obliquely scanning and step strobe lighting (OS³L) scheme for UV patterning.

As shown in Fig. 4, each UV spot has its own scanning line along the y-axis during the scanning and therefore there are $M \times N$ scanning lines within this scanning area. The average spacing between two adjacent scanning lines is Δ/N and is 8.9 nm in the case of this work. Each scanning line has its own starting point determined by the initial position of its corresponding UV spot before scanning. Let $P(i, j)$ represents the (i^{th}, j^{th}) pixel of the projected UV spots array and $\{x_0(i, j), y_0(i, j)\}_{(i=1 \sim M, j=1 \sim N)}$ be the initial coordinates of the center of $P(i, j)$ before scanning. One can easily determine these $\{x_0(i, j), y_0(i, j)\}$ coordinates based on given pixel size Δ and tilting angle θ . For the proposed OS³L algorithm for UV patterning, the DMD chip will regularly update its digital image when the scanning distance is increased by a step distance of S . Therefore, in the scanning area, there are many points at which their corresponding DMD pixels can be re-assigned to either “ON” or “OFF” depending on how to best achieve the desired distribution of UV dose. The coordinates of these points are,

$$(x_{ijk}, y_{ijk}) = (x_0(i, j), y_0(i, j) + k \cdot S), \quad (2)$$

which represents the center position of pixel $P(i, j)$ at the k^{th} step during the scan.

It should be mentioned that in the patterning area the population density (points/ μm^2) of these points with the coordinates of (x_{ijk}, y_{ijk}) given by Eq. (2) is very high and is around $N/\Delta \cdot S$. For the system developed in this work ($N = 768$ and $\Delta = 6.84 \mu\text{m}$) and for a chosen step size (S) of $10 \mu\text{m}$ used in this work, later on, the population density is 11 points within an area of $1 \times 1 \mu\text{m}^2$. It means the patterning resolution of the proposed OS³L scheme is very high and is down to the sub-micrometer scale.

Since the scanning is at a constant speed and the “ON/OFF” status of DMD pixels will remain the same within the scanning interval of distance S , the distribution of projected UV dose from an UV spot at status “ON” is the integration of $I(x, y)$ with time along the scanning interval distance of S . This means that, in comparison to the spot size defined by $I(x, y)$ as shown in Fig. 3, the area size of the projected UV dose by each DMD pixel will elongate along the scanning direction (y-axis) by a length of S , which is detrimental to the spatial resolution of UV patterning. This issue can be resolved by choosing a small value of S , but the price to pay is sacrificing the scanning speed and therefore significantly reduces the throughput of UV patterning. Therefore, a strobe lighting approach is adopted in this work. As shown in Fig. 4, the LED light source can be modulated by and synchronized with the DMD trigger signals and therefore turned into a strobe light with a duty cycle of $\mu(\%)$. For the UV exposure carried out at a constant scanning speed of v , the time interval between two adjacent DMD images is,

$$T = \frac{S}{v}. \quad (3)$$

In addition, the elementary distribution of UV dose projected by an UV spot on the PR layer is,

$$u(x, y) = \int_0^{\mu T} I_0 \cdot e^{\frac{-2(x^2 + (y - v \cdot t)^2)}{w_0^2}} dt. \quad (4)$$

By substituting $s = v \cdot t$ into Eq. (4), one has,

$$u(x, y) = \frac{1}{v} \int_0^{\mu S} I_0 \cdot e^{\frac{-2(x^2 + (y - s)^2)}{w_0^2}} ds. \quad (5)$$

This shows the projected UV dose distribution is controlled by duty cycle μ and step size S , and the magnitude of UV dose is inversely proportional to the scanning speed v . By choosing a small value of the duty cycle μ , one can limit the projected UV spot size for better pattern resolution. In the meantime, it can maintain a high scanning speed for higher patterning throughput. In this work, a 10% duty cycle is used for μ and the corresponding distribution of projected UV dose by an UV spot modeled by Eq. (1) is calculated with an assuming scanning speed of 10 mm/s. The result is shown in Fig. 5(a). The cross-sectional profiles of the calculated $u(x, y)$ along the x- and y-axis are also shown in Fig. 5(b). It shows that the projected UV dose distribution from one UV spot within one scanning step is still very close to the original UV spot under 10% strobe lighting and 10 μm step distance. The magnitude of $u(x, y)$ can be easily adjusted by changing the scanning speed v . This specific UV dose distribution in x-y space serves as a basic unit of energy package for building up the overall UV dose distribution, $U(x, y)$, on the PR layer. Mathematically, one has,

$$U(x, y) = \sum_{i,j,k}^{\text{All}} b(i, j, k) \cdot u(x - x_{ijk}, y - y_{ijk}), \quad (6)$$

where $b(i, j, k)$ is the bit value or the “ON-OFF” condition for DMD pixel $P(i, j)$ at the k^{th} step. If a point associated with the coordinate of (x_{ijk}, y_{ijk}) defined in Eq. (2) is determined to be included for UV exposure during the scanning process, then the value of $b(i, j, k)$ is 1. Otherwise, it will be 0. Once the values for all $b(i, j, k)$ are determined, the binary DMD images are also determined in the PC and will be sequentially sent to the DMD controller and DMD chip during scanning. Finally, the UV patterning algorithm is now focusing on how to properly choose the UV exposing points associated with the coordinates (x_{ijk}, y_{ijk}) such that the UV dose distribution governed by Eq. (6) can best match the target UV dose distribution, the $U^{\text{target}}(x, y)$.

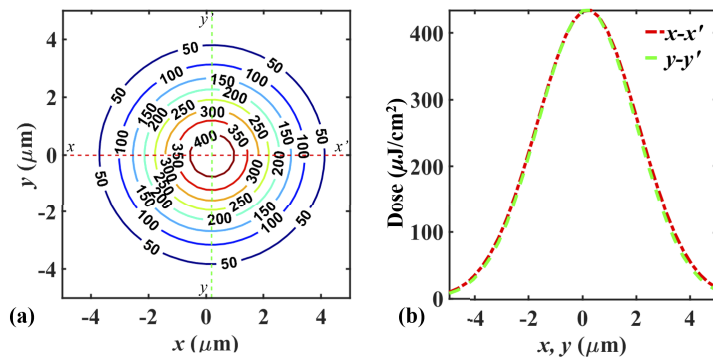


Fig. 5. (a) The calculated distribution of UV dose for an UV spot scanning at a speed of 10 mm/s along with a 10% duty cycle of strobe lighting and a step distance of 10 μm ; (b) the cross-sectional profiles of UV dose distribution along x- (red dash-dotted line) and y-axis (green dashed line).

2.4. Characteristic curve of photoresist

To determine the desired UV dose distribution of $U^{\text{target}}(x, y)$ for targeted 3D microstructures, it is necessary to first determine the characteristic curve of the PR before UV exposure and PR development. In this study, a positive photoresist (AZ P4620, Microchemicals GmbH, Ulm, Germany) is used along with the developed maskless lithography system and the proposed OS³L patterning scheme for achieving 3D microstructures from a PR layer. The characteristic curve, which gives the depth of PR being removed by PR developing processes at a given amount of exposed UV dose, is experimentally determined. The liquid AZ P4620 is uniformly spin-coated on a silicon wafer at a spinning rate of 1,000 rpm, and then soft-baked directly on a heating plate at 110 °C for 180 sec to yield a 14.7 μm thick photoresist thin layer. After UV exposure, the PR is developed in a semi-automatic developing machine (ELS706SA, ELS System Technology Co., Ltd., Hsinchu, Taiwan) using the standard developer of AZ P4620. The PR developing processes consist of six cycles. In each cycle, the developer liquid is sprayed for 5 sec and sits still on top of the PR for another 50 sec before being spun off. The above-mentioned procedures and parameters in preparing and developing the PR layers are strictly followed throughout this work to ensure consistency in experiments.

To effectively determine the characteristic curve of AZ P4620, the UV exposure is performed by the constructed DMD maskless lithography system and the grayscale functions installed inside the DMD controller. Grayscale values between 0 to 255 can be assigned to different pixels in the DMD chip such that the different levels of UV dose can be proportionally applied to the PR layer at different locations of the pixels. After PR development, the depth profiles of obtained concave PR microstructures at different dose levels can be measured for constructing the characteristic curve of AZ P4620. In experiments, a number of pixels sparsely located around the center of the DMD chip are chosen and assigned different grayscale values for UV exposure. The distribution of projected UV dose for each pixel can be directly obtained from $I(x, y)$, the total exposure time, and the corresponding grayscale value. After experimental testing, a total exposure time of 101 ms and eight DMD grayscale values of 43, 46, 53, 83, 126, 169, 212, and 255 are chosen to determine the characteristic curve. The corresponding peak UV dose at the center of the projected UV spot are 74, 78, 91, 143, 216, 290, 363 and 437 mJ/cm^2 , respectively. After PR development, the depth profiles of exposed areas from the chosen pixels are measured by laser confocal microscopy (VK-9700, Keyence Ltd., Osaka, Japan). Figure 6(a) shows the measured cross-sectional depth profiles under the eight UV dose levels. It can be seen in Fig. 6(a) that is the case with a peak dose value of 437 mJ/cm^2 , the 14.7 μm thick PR layer in the central

area has been completely removed. Based on the measured depth profiles and the UV dose, the characteristic curve of AZ P4620 is determined as shown in Fig. 6(b). A threshold of 37 mJ/cm^2 is observed in the curve.

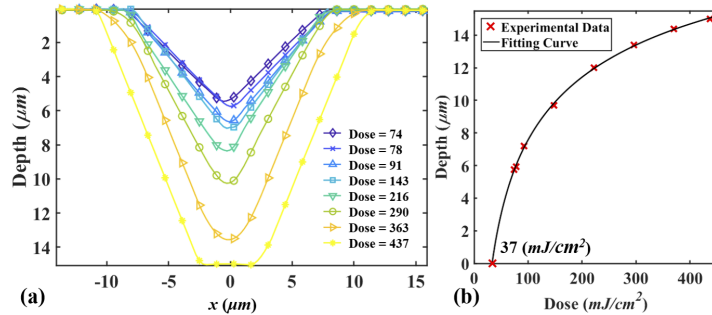


Fig. 6. (a) The measured depth profiles of developed AZ P4620 under eight different levels of UV dose, and (b) the obtained characteristic curve of AZ P4620.

3. Experiments and results

3.1. Maskless lithography and light guiding plate

To demonstrate the performance of the developed DMD-based maskless lithography system, experiments are carried out with application on light guiding plates used in the backlight modulus of the flat panel display industry. As shown in Fig. 7(a), the constructed maskless lithography system is first applied for UV patterning a $14.7 \mu\text{m}$ thick AZ P4620 PR layer deposited on an 8" silicon wafer. After PR development, millions of concave microstructures of a pre-designed 3D profile and pre-determined locations are formed in the PR layer. A metal (usual nickel) mold is then negatively replicated by electroforming from the fabricated PR microstructures, as shown in Fig. 7(b). Finally, the metal mold can transfer its surface to a light guiding plate by either imprinting or injection molding processes. As shown in Fig. 7(c), light coming from discrete light sources (such as LEDs) on the edge of the plate can be re-directed by distributed microstructures and then emitted from the surface of the light-guiding plate. To achieve this type of panel lighting with specific lighting effectiveness and illuminating uniformity, the geometrical profile and the population density of these distributed 3D surface microstructures are first designed and simulated. Various methods such as ultra-precision machining, laser ablation, etc., have been developed for fabricating these 3D microstructures.

In this study, two types of axially symmetrical 3D microstructures are chosen for maskless lithography UV patterning with applications on light guiding plates. The axially symmetric depth profiles as functions of radius (r) for type I and type II microstructures are expressed as,

$$D_I(r) = \begin{cases} 14.7 & ,0 \leq r \leq 3 \\ 14.7 - 0.6682 \cdot (r - 3) & ,3 \leq r \leq 25. \end{cases} \quad (7a)$$

$$D_{II}(r) = \begin{cases} 14.7 & ,0 \leq r \leq 5 \\ (r - 30) \cdot (-0.0018r^2 + 0.0633r - 0.8595) & ,5 < r \leq 30. \end{cases}$$

The cross-sectional profiles of type I and II microstructures are shown in Fig. 8(a) and 8(b), respectively, which have a truncated conical shape and a nozzle shape. In both cases, the total

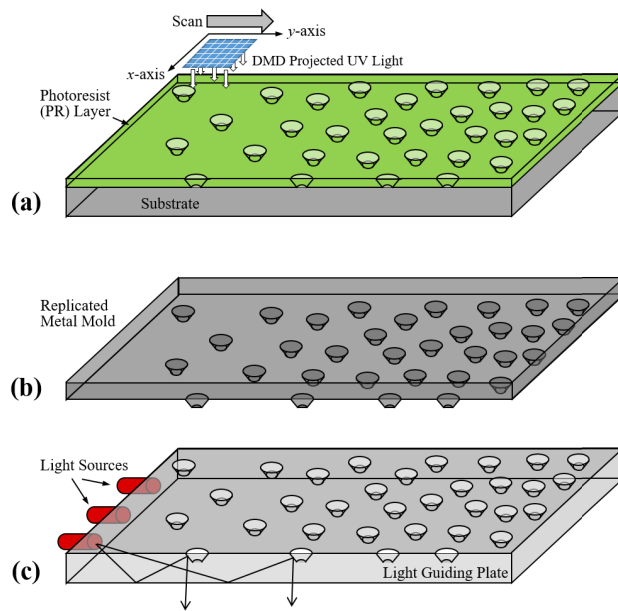


Fig. 7. Application of maskless lithography on light guiding plate; (a) concaves microstructures in a PR layer by UV patterning and PR developing, (b) metal mold replicated from PR microstructures, (c) edge-type light guiding plate for panel lighting based on distributed surface microstructures transferred from the metal mold.

numbers and the center locations of all the microstructures used for the light guiding plate were pre-determined and provided by a local company after numerical simulation. In either case, all the targeted microstructures for a light guiding plate have the same depth profile but different center locations. For a given depth profile, the corresponding distribution of UV dose can be easily determined from the PR's characteristic curve shown in Fig. 6(b). The remaining issue is how to select a specific group of UV exposing points surrounding the center of the microstructure such that the targeted UV dose distribution can be achieved after convoluting these UV exposing points with their projected UV dose distribution, as given by Eq. (6).

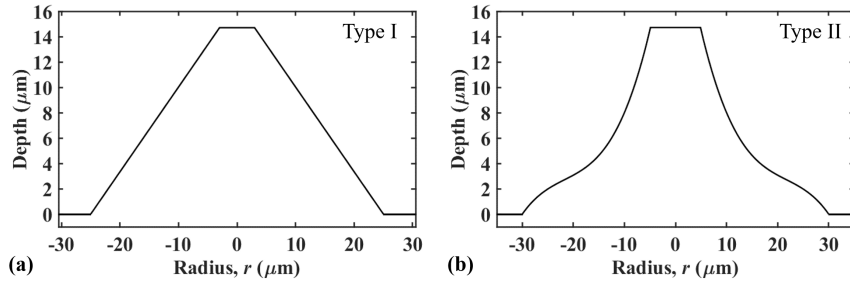


Fig. 8. Axially symmetrical depth profiles as functions of radius (r) for (a) type I and (b) type II microstructures used in maskless lithography UV patterning for light guiding plate.

3.2. Axially symmetrical UV patterning

It is noticed that the targeted 3D profiles are axially symmetric and the elementary distribution of the projected UV dose of an UV spot is also very close to axially symmetric as described in

Section 2.3 and displayed in Fig. 5(a) and 5(b). Therefore, the UV exposing points selected for UV patterning one single microstructure can also be axial-symmetrically distributed around the center position of a targeted microstructure. Let $D(r)$ be the population density of the chosen UV exposing points and $N(r)$ be the total number of points that are included within a radius of r from the center, one has,

$$N(r) = 2\pi \int_0^r D(\xi) \cdot \xi \cdot d\xi. \quad (8)$$

If all the points are restricted from a maximum radius of r_0 and the total number of points being selected for constructing the desired UV dose distribution of a target microstructure is N_0 , one has,

$$N_0 = 2\pi \int_0^{r_0} D(\xi) \cdot \xi \cdot d\xi. \quad (9)$$

For a given $D(r)$, the coordinates of the UV exposing points which are axial-symmetrically distributed around the center can be numerically generated. With the given coordinates of these points, the overall distribution of UV dose can be calculated by Eq. (6). The expected depth profile can be determined from PR's characteristic curve and compared with the targeted depth profile. Numerical iteration is then carried out to find out the best choice of $D(r)$ which can minimize the difference between the simulated depth profile and the targeted one. To fulfill this iterating process, the $D(r)$ is first represented by a N th-order polynomial as,

$$D(r) = \sum_{i=0}^N a_i \cdot r^i. \quad (10)$$

The Nelder-Mead simplex algorithm [47], which is a minimization algorithm for a function of multiple variables, is adopted here for numerically determining the best choices of a_i , r_0 , and v , which can result in the target depth profile after UV patterning and PR developing.

Numerical simulation and optimization of the parameters are carried out for both type I and II microstructures and the obtained results are shown in Table 1. An 8th-order polynomial is used for $D(r)$. The duty cycle of strobe lighting (μ) is kept as 10% without changing. The optimized maximum radius of distributed points is 25.80 μm and 30.98 μm for type I and II microstructure, respectively, and the suggested scanning speed is 15.49 mm/s and 12.34 mm/s, respectively. Based on the obtained $D(r)$, the distributed UV exposing points for UV patterning one single targeted microstructure are shown in Fig. 9(a) and 9(b) for type I and II microstructures, respectively. The UV dose distribution is then calculated by Eq. (6) with the coordinates of these points. Simulated depth profiles are then obtained with the PR's characteristic curve shown in Fig. 6(b). The contour plots and the cross-sectional profiles of simulated depth profiles are shown in Fig. 10(a) and 10(b), respectively, for both types of microstructures. Also shown in Fig. 10(b) with dashed lines are the targeted depth profiles. It is noticed that the simulated profiles can well match the targeted ones with good accuracy and major discrepancies are observed when the depth is small and close to zero. This is understood by the steep rising of developed PR depth around the threshold of UV dose in the PR's characteristic curve as shown in Fig. 6(b).

3.3. Experimental results

With the coordinates of UV exposing points for one single microstructure being given and shown in Fig. 9, the developed DMD-based maskless lithography system and its OS³L UV patterning scheme are now ready for fabricating all the targeted 3D microstructures for a light-guiding plate. Since the center positions of targeted microstructures are already known, the expected coordinates of all the UV exposing points are also determined. As mentioned in Sec. 2.C, the population density of all the available UV exposing points with their coordinates (x_{ijk}, y_{ijk}) given by Eq. (2) is very high and is approximately 11 points/ μm^2 . Therefore, for each numerically

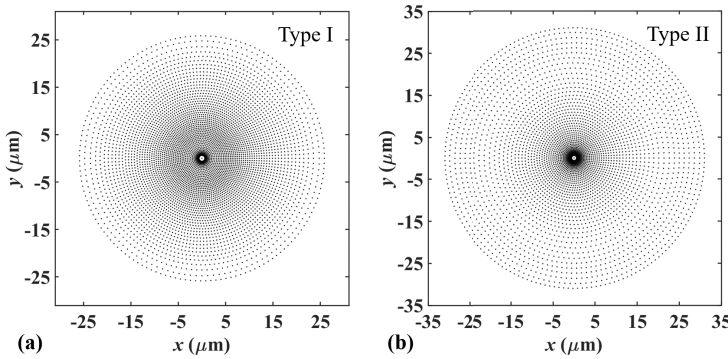


Fig. 9. The distribution of UV exposing points for (a) type I and (b) type II microstructures.

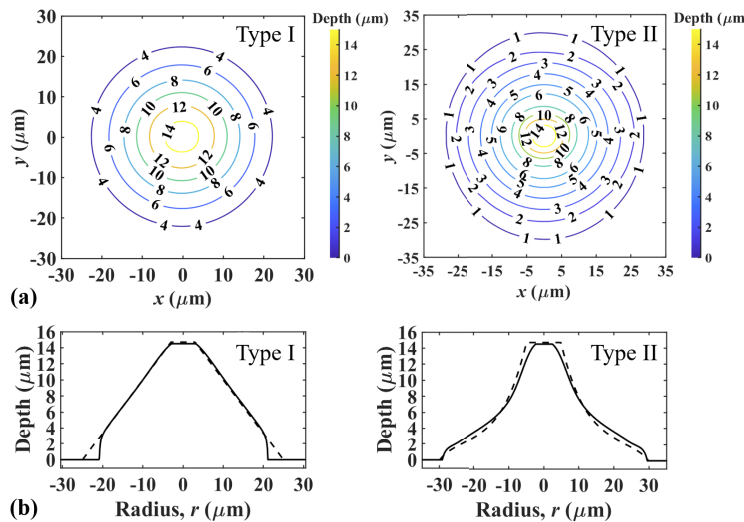


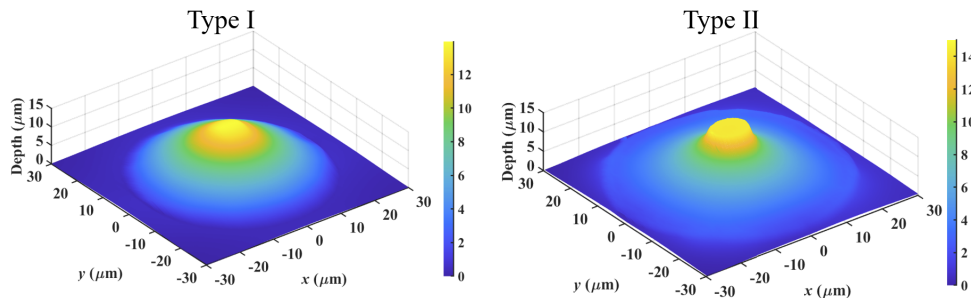
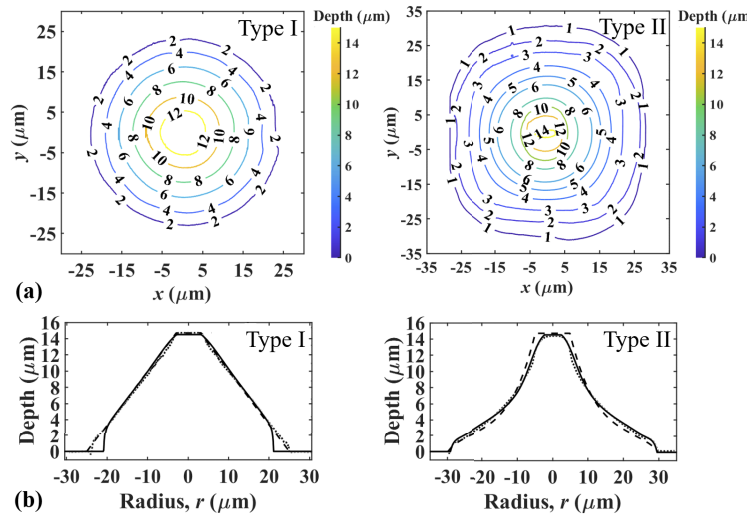
Fig. 10. (a) Contour plots and (b) cross-sectional plots of simulated depth profiles for type I and II microstructures. Targeted depth profiles are shown with dash lines in (b) for comparison.

simulated exposing point, it is always possible to find its corresponding UV exposing point from (x_{ijk}, y_{ijk}) with a minimized position error less than 200~300 nm. This small position error is always existing when picking up the UV exposing points for UV patterning. However, it should have a very limited effect on the finally achieved depth profile since it is much smaller than the dimensional sizes of the targeted microstructures.

Fig. 11 and Fig. 12 show the experimental results of the fabricated Type I and II microstructures. The experiments are carried out on a 14.7 μm thick PR (AZ P4620) layer deposited on an 8" Si wafer. All the material processing parameters and the maskless UV exposing parameters are strictly following what has been given in before. Figure 11 shows the measured 3D depth profiles of Type I and II PR microstructures, respectively, after being fabricated by UV patterning and PR development. Figure 12(a) shows the same depth profiles but in contour plots so that one can compare them with the simulated ones shown in Fig. 10(a). The cross-sectional depth profiles of experimentally fabricated microstructures are shown in Fig. 12(b) in dot lines and, for the purpose of comparison, the targeted profiles are also shown in dash lines. One can see that very good agreement are achieved.

Table 1. Optimized results for depth profile of type I and type II

Type	I	II
v (mm/s)	15.49	12.34
μ (%)	10	10
r_0 (μm)	25.80	30.98
a_0	2855.895	2382.336
a_1	-2645.663	-1395.56
a_2	1221.738	483.146
a_3	-250.082	-92.51
a_4	28.423	9.484
a_5	-1.912	-0.7826
a_6	0.0777	0.03094
a_7	-0.001708	-0.00004038
a_8	0.0000158	0.0000032
Iteration Numbers	137	176

**Fig. 11.** 3D plots of the depth profiles of fabricated Type I and Type II concave microstructures after UV patterning and PR development.**Fig. 12.** (a) Contour plots and (b) cross-sectional plots of the depth profiles of experimentally fabricated type I and type II microstructures. Targeted depth profiles are shown with dash lines in (b) for comparison.

The experimental result of large-area patterning of microstructures on a PR-coated 8" wafer is shown in Fig. 13. In this case, the type I microstructures are used as an example and the fabricated PR concave microstructures will be used for replicating a metal (nickel) mold for subsequent manufacturing of light guiding pates. The overall patterning area is rectangular with 160 mm in length and 115 mm in width. With a scanning speed of 15.49 mm/s given in Table 1, it took 11 seconds for the maskless lithography system to finish one scan along the length direction. Since the width of projected DMD image is around 7 mm, there are totally 19 scans to complete the whole patterning area with 1 mm over lapping between two adjacent scans. The total UV patterning time by the maskless lithography system on this $160 \times 115 \text{ mm}^2$ area is less than 4 minutes. This is very high throughput.

A number of optical microscope (OM) images taken at different locations of the patterning area are shown in Fig. 13(a) to 13(k). The concave PR microstructures are randomly and uniformly distributed within a localized area. However, the density of the fabricated microstructures is different according to a pre-determined design. The filling ratio, which is defined as the percentage of the occupied surface area of fabricated microstructures within a given area, can be as high as 70.5% such as examples shown in Fig. 13(a) and 13(c). Even with such a high filling ratio, all the fabricated microstructures are still intact and distinct with each other. It indicates the patterning accuracy of the developed DMD-based maskless lithography system. Figure 14 shows several scanning electron microscope (SEM) images at different scales of the fabricated concave microstructures in PR layer. Smooth surface profiles with excellent uniformity

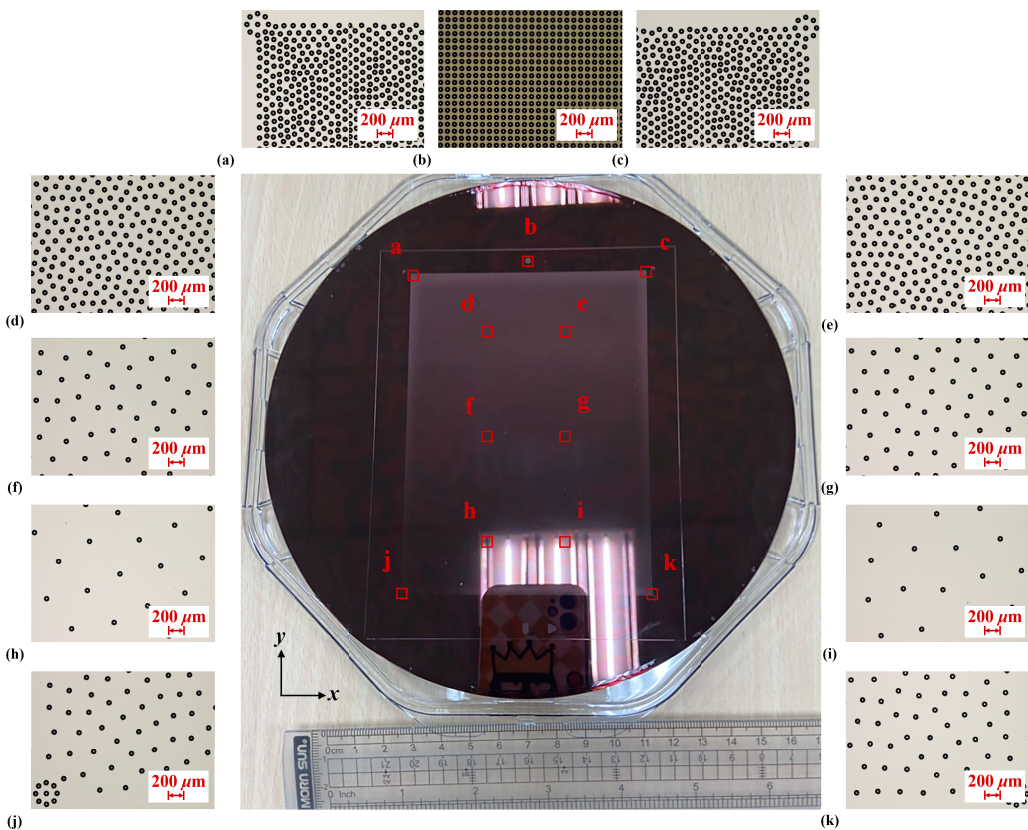


Fig. 13. Photo and optical microscope images of the fabricated PR microstructures on an 8" silicon wafer.

are observed, which again demonstrates the capability of the proposed DMD-based maskless lithography system and its potential for large-area patterning of 3D microstructures.

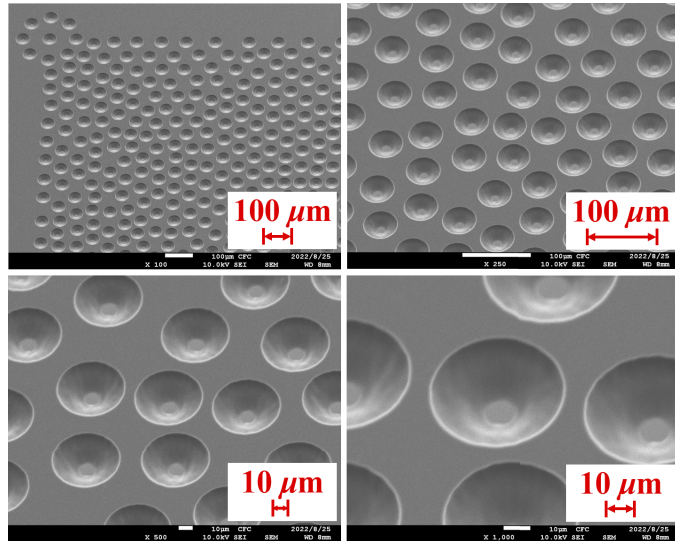


Fig. 14. SEM images of fabricated 3D microstructures in a PR layer with the application as a mother mold for light guiding plate.

4. Conclusions

In this paper we reported the development of a DMD-based maskless lithography system and its UV patterning scheme based on the obliquely scanning and step strobe lighting method. The digital image consisted of arrayed UV spots and defined by a DMD chip is projected by a 0.5x imaging lens onto a PR layer for UV exposure. The projected UV light mechanically scans over the PR layer strip by strip in a stitching manner to finally achieve a targeted spatial distribution of UV dose. After PR developing, patterned microstructures with targeted 3D profiles can be obtained. Efforts are placed on improving patterning resolution and maintaining higher patterning speed so that this system can be used for large area fabrication of 3D microstructures. The procedures for determining the binary DMD images which are sequentially applied to the DMD chip in a synchronized manner with the scanning movements is also provided. It requires experimental data of the irradiance of a projected UV spots as well as the characteristic curve of the PR layer during UV exposure and developing. Numerical simulation and optimization algorithm are also utilized to bring the projected UV dose distribution closer to the targeted one and therefore to achieve precise control on the fabricated microstructures.

Experiments have been successfully carried out on a 14.7 μm thick AZ P4620 PR layer deposited on an 8" Si wafer. The targeted concave microstructures have truncated conical and nozzle-shaped profiles with aperture sizes around 50 to 60 μm at one end and 6 to 10 μm at the other end. Millions of these targeted microstructures with pre-determined positions have been fabricated on the PR layer in an area size of $160 \times 115 \text{ mm}^2$. These patterned microstructures have a pre-designed population density distribution varied from 2.6% to 70.5% and can be used as the mother mold for subsequent production of light guiding plates. The total time for the complete UV patterning is only 4 minutes.

The proposed maskless lithography system and its UV patterning scheme are very versatile, flexible, and powerful. It can balance the performance specifications by adopting different

combination of duty cycle (μ), step distance (S), and scanning speed (v). It can be easily adjusted for fabricating many kinds of concave and/or convex microstructures with axial-symmetrical, non-axial-symmetrical, or even free-formed surface profiles. It can be applied to expose both positive and negative PRs of different layer thicknesses as along as the PR's exposure-developing characteristics are under controlled. To deal with even smaller microstructures or to achieve better accuracy in UV patterning, one can use DMD chips with smaller pixel size, for examples, 7.56 μm in the 0.65" or 0.9" DMD chips (DLP6500 or DLP9000, TI, TX, USA). It will reduce the projected UV spot size by almost one half and hence significantly improve the resolution in UV patterning. One can also utilize an imaging projection lens with a higher de-magnifying factor to reduce the projected UV spot size. However, it will also shrink the overall area size of projected UV image and hence decrease the patterning throughput. In short, there are many possibilities and opportunities for engineering and industry applications, and related investigations are under way.

Funding. Ministry of Science and Technology, Taiwan (111-2622-E-006-025).

Acknowledgments. This research was supported by the Southern Taiwan Science Park Bureau, Ministry of Science and Technology, Taiwan, R.O.C. under contract no. 111CP-2-01.

Disclosures. The authors declare no conflicts of interest.

Data availability. Data underlying the results presented in this paper are not publicly available at this time but may be obtained from the authors upon reasonable request.

References

1. R. Henderson, R. Pease, A. Voshchenkov, R. Helm, and R. Wadsack, "A high-speed p-channel random access 1024-bit memory made with electron lithography," *IEEE J. Solid-State Circuits* **10**(2), 92–96 (1975).
2. H. Yasuda, T. Haraguchi, H. Yabara, K. Takahata, H. Murata, E. Rokuta, and H. Shimoyama, "Multiaxis and multibeam technology for high throughput maskless e-beam lithography," *J. Vac. Sci. Technol., B: Nanotechnol. Microelectron.: Mater., Process., Meas., Phenom.* **30**(6), 06FC01 (2012).
3. H. Kueck, M. Bollerott, W. Doleschal, A. Gehner, W. Grundke, D. Kunze, R. Melcher, J. Paufler, R. Seltmann, and G. Zimmer, "New system for fast submicron laser direct writing," in *Optical/Laser Microlithography VIII*, vol. 2440 T. A. Brunner, ed., International Society for Optics and Photonics (SPIE, 1995), pp. 506–514.
4. R. Barbucha, M. Kocik, J. Mizeraczyk, G. Koziol, and J. Borecki, "Laser direct imaging of tracks on pcr covered with laser photoresist," *Bull. The Pol. Acad. Sci. Sci.* **56**, 17–20 (2008).
5. B. Du, H. Zhang, J. Xia, J. Wu, H. Ding, and G. Tong, "Super-resolution imaging with direct laser writing-printed microstructures," *The Journal of Physical Chemistry A* **124**(35), 7211–7216 (2020).
6. D. J. D. Carter, D. Gil, R. Menon, M. K. Mondol, H. I. Smith, and E. H. Anderson, "Maskless, parallel patterning with zone-plate array lithography," *J. Vac. Sci. Technol. B* **17**(6), 3449–3452 (1999).
7. D. Gil, R. Menon, and H. I. Smith, "The case for diffractive optics in maskless lithography," *J. Vac. Sci. Technol. B* **21**(6), 2810–2814 (2003).
8. R. Menon, A. Patel, E. E. Moon, and H. I. Smith, "Alpha-prototype system for zone-plate-array lithography," *J. Vac. Sci. Technol. B* **22**(6), 3032–3037 (2004).
9. DLP® 0.7 XGA 2xLVDS TYPE-A DMD, <https://www.ti.com/product/DLP7000>. Accessed: 2022-10-16.
10. K. Takahashi and J. Setoyama, "A uv-exposure system using dmd," *Electron. Comm. Jpn. Pt. II* **83**(7), 56–58 (2000).
11. R. Yang, K. Chan, Z. Feng, I. Akihito, and W. Mei, "Design and fabrication of microlens and spatial filter array by self-alignment for maskless lithography systems," *J. Microlithogr. Microfabr. Microsystems* **2**, 26 (2003).
12. K. Chan, Z. Feng, R. Yang, A. Ishikawa, and W. Mei, "High-resolution maskless lithography," *J. Microlithogr. Microfabr. Microsystems* **2**(4), 331 (2003).
13. J. Wang, Y. Hayasaki, F. Zhang, X. Wang, and S. Sun, "Variable scattering dots: Laser processing light guide plate microstructures with arbitrary features and arrangements," *Opt. Laser Technol.* **136**, 106732 (2021).
14. J. wang jianfei dong, "Design of flexible optical waveguide with high uniformity and efficiency for light therapies," *Opt. Lasers Eng.* **151**, 106933 (2022).
15. M. Jakubowsky, J. Werder, C. Rytka, P. M. Kristiansen, and A. Neyer, "Correction to: Design, manufacturing and experimental validation of a bonded dual-component microstructured system for vertical light emission," *Microsyst. Technol.* **27**(5), 2237 (2021).
16. Y.-B. Lee, G.-W. Yoon, and J.-B. Yoon, "Mass-producible structural design and fabrication method for a slim light-guide plate having inverse-trapezoidal light out-couplers," *J. Micromech. Microeng.* **29**(3), 035001 (2019).
17. H.-X. Yin, C.-R. Zhu, Y. Shen, H.-F. Yang, Z. Liu, C.-Z. Gu, B.-L. Liu, and X.-G. Xu, "Enhanced light extraction in n-gan-based light-emitting diodes with three-dimensional semi-spherical structure," *Appl. Phys. Lett.* **104**(6), 061113 (2014).

18. C. M. Waits, A. Modafe, and R. Ghodssi, "Investigation of gray-scale technology for large area 3d silicon MEMS structures," *J. Micromech. Microeng.* **13**(2), 170–177 (2002).
19. N. Y. J. Tan, X. Zhang, D. W. K. Neo, R. Huang, K. Liu, and A. Senthil Kumar, "A review of recent advances in fabrication of optical fresnel lenses," *J. Manuf. Process.* **71**, 113–133 (2021).
20. Y. Liang, T. Zhu, M. Xi, H. N. Abbasi, J. Fu, R. Su, Z. Song, H. Wang, and K. Wang, "Fabrication of a diamond concave microlens array for laser beam homogenization," *Opt. Laser Technol.* **136**, 106738 (2021).
21. W. Yuan, Y. Cai, C. Xu, H. Pang, A. Cao, and Q. Deng, "Fabrication of multifocal microlens array by one step exposure process," *Micromachines* **12**(9), 1097 (2021).
22. X. Zhang, Z. Chen, J. Chen, Z. Wang, and L. Zhu, "Fabrication of a microlens array featuring a high aspect ratio with a swinging diamond tool," *J. Manuf. Process.* **75**, 485–496 (2022).
23. L. Giorleo, E. Ceretti, and C. Giardini, "Optimization of laser micromachining process for biomedical device fabrication," *Int. J. Adv. Manuf. Technol.* **82**(5-8), 901–907 (2016).
24. J.-J. Kim, S.-P. Yang, D. Keum, and K.-H. Jeong, "Asymmetric optical microstructures driven by geometry-guided resist reflow," *Opt. Express* **22**(18), 22089–22094 (2014).
25. J. Jin, S. Di, W. Lin, and X. Wang, "Simulation and optimization of microlens hot-melting fabricating process based on finite element method," *Microelectron. Eng.* **250**, 111634 (2021).
26. H. Zhang, T. Qi, X. Zhu, L. Zhou, Z. Li, Y.-F. Zhang, W. Yang, J. Yang, Z. Peng, G. Zhang, F. Wang, P. Guo, and H. Lan, "3d printing of a pdms cylindrical microlens array with 100% fill-factor," *ACS Appl. Mater. Interfaces* **13**(1), 1–17 (2021).
27. M. Seo and H. Kim, "Lithography upon micromirrors," *Comput. Des.* **39**(3), 202–217 (2007).
28. Y. Watanabe, H. Kono, Y. Kanaya, Y. Saito, T. Sakamoto, S. Owa, N. Hirayamagi, T. Koo, C. Poppe, D. Tseng, C. Sorensen, H. Lee, S. Renwick, and B. Yuan, "Digital scanner, optical maskless exposure tool with DUV solid state laser," in *Optical Microlithography XXXIV*, vol. 11613 S. Owa and M. C. Phillips, eds., International Society for Optics and Photonics (SPIE, 2021), p. 1161309.
29. J. Choi, G. Kim, W.-S. Lee, W. S. Chang, and H. Yoo, "Method for improving the speed and pattern quality of a dmd maskless lithography system using a pulse exposure method," *Opt. Express* **30**(13), 22487–22500 (2022).
30. K. Zhong, Y. Gao, F. Li, N. Luo, and W. Zhang, "Fabrication of continuous relief micro-optic elements using real-time maskless lithography technique based on dmd," *Optics & Laser Technology* **56**, 367–371 (2014).
31. S.-I. Bae, K. Kim, S. Yang, K. won Jang, and K.-H. Jeong, "Multifocal microlens arrays using multilayer photolithography," *Opt. Express* **28**(7), 9082–9088 (2020).
32. K.-Y. Hung and T.-H. Liang, "Application of inclined-exposure and thick film process for high aspect-ratio micro-structures on polymer optic devices," *Microsyst. Technol.* **14**(9-11), 1217–1222 (2008).
33. G. Jiang, S. Baig, and M. R. Wang, "Prism-assisted inclined UV lithography for 3d microstructure fabrication," *J. Micromech. Microeng.* **22**(8), 085022 (2012).
34. S. F. Shiba, K. Wang, and J. J. Kim, "Tilted uv-led lithography for 3d microfabrication," in *in 2021 21st International Conference on Solid-State Sensors, Actuators and Microsystems (Transducers)*, (2021), pp. 517–520.
35. K. Y. Kwon, A. Weber, and W. Li, "Varying-length polymer microneedle arrays fabricated by droplet backside exposure," *J. Microelectromech. Syst.* **23**(6), 1272–1280 (2014).
36. A. Kaltashov, P. K. Parameshwar, N. Lin, and C. Moraes, "Accessible, large-area, uniform dose photolithography using a moving light source," *J. Micromech. Microeng.* **32**(2), 027001 (2022).
37. M. A. Smith, S. Berry, L. Parameswaran, C. Holtsberg, N. Siegel, R. Lockwood, M. P. Chrisp, D. Freeman, and M. Rothschild, "Design, simulation, and fabrication of three-dimensional microsystem components using grayscale photolithography," *J. Micro/Nanolithogr., MEMS, MOEMS* **18**(04), 1 (2019).
38. L. Mosher, C. Waits, B. Morgan, and R. Ghodssi, "Double-exposure grayscale photolithography," *J. Microelectromech. Syst.* **18**(2), 308–315 (2009).
39. B. Badawi, O. Sayadi, I. Eisele, and C. Kutter, "Three-state lithography model: an enhanced mathematical approach to predict resist characteristics in grayscale lithography processes," *J. Micro/Nanopattern. Mats. Metro.* **20**(01), 1 (2021).
40. Y. Hirai, K. Sugano, T. Tsuchiya, and O. Tabata, "A three-dimensional microstructuring technique exploiting the positive photoresist property," *J. Micromech. Microeng.* **20**(6), 065005 (2010).
41. X. Ma, Y. Kato, F. Kempen, Y. Hirai, T. Tsuchiya, F. Keulen, and O. Tabata, "Multiple patterning with process optimization method for maskless dmd-based grayscale lithography," *Procedia Eng.* **120**, 1091–1094 (2015).
42. A. Rammohan, P. K. Dwivedi, R. Martinez-Duarte, H. Katepalli, M. J. Madou, and A. Sharma, "One-step maskless grayscale lithography for the fabrication of 3-dimensional structures in su-8," *Sens. Actuators, B* **153**(1), 125–134 (2011).
43. H. Chien and Y. Lee, "Three dimensional maskless ultraviolet exposure system based on digital light processing," *Int. J. Precis. Eng. Manuf.* **21**(5), 937–945 (2020).
44. M. N. Hasan, D. Duc Hanh, H.-L. Chien, and Y.-C. Lee, "Maskless beam pen lithography based on integrated microlens array and spatial-filter array," *Opt. Eng.* **56**(11), 1 (2017).
45. D.-H. Dinh, H.-L. Chien, and Y.-C. Lee, "Maskless lithography based on digital micromirror device (dmd) and double sided microlens and spatial filter array," *Opt. Laser Technol.* **113**, 407–415 (2019).
46. H.-L. Chien, Y.-H. Chiu, and Y.-C. Lee, "Maskless lithography based on oblique scanning of point array with digital distortion correction," *Opt. Lasers Eng.* **136**, 106313 (2021).
47. J. A. Nelder and R. Mead, "A simplex method for function minimization," *Comput. J.* **7**(4), 308–313 (1965).